This article has been accepted for publication in a future issue of this journal, but has not been fully edited. Content may change prior to final publication. Citation information: DOI 10.1109/TSG.2022.3150226, IEEE Transactions on Smart Grid



# Self-Organizing Map-Based Resilience Quantification and Resilient Control of Distribution Systems Under Extreme Events

Kumar Utkarsh, *Member, IEEE*, and Fei Ding, *Senior Member, IEEE*

***Abstract*— Due to climate change, extreme weather events are occurring more frequently and with increasing impact. This trend poses a significant challenge for distribution system operators (DSO) to ensure that there is uninterrupted power supply to critical loads in their networks. To embed resilience into DSO's decision-making, resilience needs to be first quantified and then integrated into the system-level optimization. Therefore, this paper first develops a novel self-organizing map (SOM) based method (called SomRes) to quantify the time-varying resilience index of a system that can leverage the powerful classification property of SOMs and removes some of the disadvantages of subjective weight assignment methods. Using SomRes, a resilient resource allocation and operational dispatch algorithm is further developed to enhance system resilience against extreme events by considering the SomRes resilience index directly as the feedback. The proposed resilience quantification approach is benchmarked with a state-of-the-art approach and the efficacy of the proposed resilient dispatch algorithm is demonstrated through several deterministic and statistical case studies on the IEEE 123-bus distribution system. Simulation studies show that the proposed SomRes quantification method is an appropriate indicator of system resilience, and the resilient resource allocation and dispatch strategy can significantly reduce critical load shedding under varying event propagation scenarios.**

***Index Terms*—distributed energy resource, grid resilience, model predictive control, self-organizing maps.**

## NOMENCLATURE

***Abbreviations***

| | |
|---|---|
| BESS | Battery energy storage system |
| CI | Choquet integral |
| DER | Distributed energy resource |
| DG | Diesel generator |
| DSO | Distribution system operator |
| LEMS | Load energy management system |
| MPC | Model-predictive control |
| PCC | Point of common coupling |
| PV | Photovoltaic system |
| RE | Resilience-enhanced |
| RN | Resilience-neutral |
| SOM | Self-organizing map |
| SOC | State of charge of a BESS |
| UAV | Unmanned autonomous vehicle |

***Constants***

| | |
|---|---|
| $T$ | Set of T time-steps indicating optimization horizon |
| $N$ | Number of nodes in the system |
| $N_S$ | Number of neurons in the SOM model |
| $\tilde{v}_0$ | Squared nominal voltage in per unit |
| $\hat{g}_i$ | Max capacity of the generation asset at node $i$ |
| $\hat{l}_i^c$ | Max critical load requirement at node $i$ |
| $v_{min}, v_{max}$ | Lower, upper limit of allowable node voltages |
| $p_{pv,n,0}^t$ | Max available power at time $t$ of the PV at node $n$ |
| $\alpha_{ch}, \alpha_{dis}$ | Charge/discharge efficiency of all BESS |
| $p_{bat,max}^n$ | Max (dis)charge power of BESS at node $n$ |
| $I_{bat}^n$ | kVA capacity of BESS inverter at node $n$ |
| $S_{min}^n, S_{max}^n$ | Limits on remaining energy of BESS at node $n$ |
| $D_n^0$ | Initial diesel availability at a DG node $n$ |
| $T_e$ | Set of edges (or roads) in the transportation network |
| $r_n^i$ | $i^{th}$ road connecting a node $n$ |
| $p_{n,0}^{max}, p_{n,0}^{min}$ | Max and min capacity of the DG at node $n$ |
| $\pi$ | Coefficients for SOM linear regression |
| $\gamma_*$ | General notation for weights in an objective function |
| $S$ | Set of event propagation scenarios |

***Variables***

| | |
|---|---|
| $p_{n,*}^t, q_{n,*}^t$ | Nominal active/reactive power of LEMS $n$ at time $t$ |
| $p_{n,\wedge}^t, q_{n,\wedge}^t$ | Upper bound of LEMS powers at node $n$ at time $t$ |

Kumar Utkarsh and Fei Ding are with the National Renewable Energy Laboratory, Golden, CO 80401 USA (Corresponding Author: Fei Ding, fei.ding@nrel.gov). This work was authored by the National Renewable Energy Laboratory, operated by Alliance for Sustainable Energy, LLC, for the U.S. Department of Energy (DOE) under Contract No. DE-AC36-08GO28308. Funding provided by the Laboratory Directed Research and Development (LDRD) program. The views expressed in the article do not necessarily represent the views of the DOE or the U.S. Government. 

| | |
|---|---|
| $p_{n,\vee}^t, q_{n,\vee}^t$ | Lower bound of LEMS powers at node *n* at time *t* |
| $g_i(t)$ | Generation asset dispatch at node *i* at time *t* |
| $p_{n,*}^t, q_{n,*}^t$ | Optimal power setpoints to LEMS *n* at time *t* |
| $v_n^t$ | Estimated voltage at node *n* at time *t* |
| $p_{pv,n}^t, q_{pv,n}^t$ | Optimal active/reactive power of PV at node *n* |
| $p_{bat,n}^t, q_{bat,n}^t$ | Optimal active/reactive power of BESS at node *n* |
| $dn_0^t$ | Diesel consumption by the DG at node *n* |
| $dn_{r^i}^t$ | Diesel transported out of node *n* through road $r^i$ |
| $b_{s,ij}^t$ | Binary value of the status of the switch $s_{ij}$ |
| $\check{A}, \hat{A}$ | Time-varying adjacency matrices of the system |
| $\psi^t$ | State vector of the system at time *t* |
| $C^t$ | Normalized critical energy served corresponding to the state $\psi^t$ over *S* event scenarios |

## I. INTRODUCTION

An important objective of electric power systems is to absorb and recover from high-consequence or damaging events [1], which defines the system's resilience. Per the report by the U.S. National Academy of Science [2], resilience can be defined as "the ability to prepare and plan for, absorb, recover from, or more successfully adapt to actual or potential adverse events." According to this definition, resilience can be categorized further as short- and long-term resilience [3]. Short-term resilience defines the features a system should have before and during an event and relates to the system's ability to resist and adapt dynamically to such events. Long-term resilience typically involves comprehensive studies considering various event propagation scenarios and planned infrastructure improvements to mitigate the effects of such events. Thus, redundancy, resources to mitigate damages, and system restoration during and after extreme events constitute some important features of the short-term resilience of a system. Short-term resilience is also the focus of this paper and is henceforth represented simply by the term "resilience".

Multiple studies have been performed to quantify and improve the resilience of power systems. These studies can be broadly divided into probabilistic and analytical categories. Under the probabilistic category, the studies employ approaches to determine the probability or the confidence interval that a system is working as intended in scenarios of damaging or catastrophic events. These studies typically peruse historic outage as well as restoration data and system parameters to determine indices affecting resilience, such as the time taken for a certain level of restoration and the speed of restoration. The resilience of a power distribution system in terms of its infrastructure, its physical environment, and restoration of service provided by the utility is evaluated in [4] based on historical data, and correlations among several factors are analyzed to determine an increase/decrease in system resilience. In [5], a probabilistic modelling method is used for resilience evaluation by including an event model, a fragility model for equipment, a system performance model, and a system restoration model; whereas [6] aims to quantify resilience using reliability component importance measures, which describe the sensitivity of the network to changing parametric conditions. The resilience is then quantified based on the property of the network to provide services.

Under the analytical category are studies in which simulations are performed with different event scenarios and the performance of the system is then assessed analytically. There are two further sub-categories under the analytical category. The first is the complex-network sub-category, which is based mainly on studying the network graph of the power distribution system and determining key parameters affecting the electrical infrastructure resilience. A multi-criteria decision-making approach is presented in [7], and the CI method is employed to quantify power system resilience using a set of influential parameters based on graph theory. In [8], a resilience evaluation framework based on supply availability to critical loads is presented incorporating not only the traditional complex network approach but also concepts such as the brittleness, dependency, and interdependency of the distribution system components. An analytical hierarchical process approach is presented to select the most influential parameters affecting resilience, and in conjunction with percolation theory, a composite resilience metric is developed in [9]. The second sub-category is that of power-flow approaches. A three-level attack model is presented in [10] to determine system hardening and restoration measures in different attack scenarios to enhance distribution system resilience. In [11] and [12], a distribution system design problem is solved using a two-stage stochastic mixed-integer programming, where the first stage solves for hardening measures and the second stage evaluates costs during extreme events. Resilience is then evaluated based on the reduction in load shedding and repair costs.

Unlike reliability, there are no universally agreed-upon indices to judge the resilience of a system, and utilities develop resilience metrics mostly depending on their own requirements and learnings [1], [2]. To fill such research gap, this paper proposes a SOM-based data-driven approach (named SomRes) that considers a diverse range of parameters to evaluate the resilience of distribution systems. The proposed approach aims to overcome the following gaps existing in resilience quantification, namely:

1) Most studies quantify the resilience of a system after an event has occurred, using the data available from that event; however, this post-event resilience quantification can inform only future planning decisions. Instead, estimating resilience of a system without depending on historical event data is critical to inform real-time decision-making both before and during an event. Therefore, in this paper, resilience is estimated using the system's present and forecasted state, such as load requirement, generation forecast, and topology information.

2) Among the few quantification techniques that do not depend on post-event data, the set of system features that they consider is very limited. Also, they might not be applicable for real-time decision-making because they require a fair amount of computation capability. On the other hand, in this paper, a data-driven quantification method is proposed based on SOM,

which can be trained offline, and the system's resilience at any time interval can be estimated by simply finding the neuron which is closest to the system features at that time.

3) Further, and importantly, existing methods, such as weighted-sum or CI-based methods, need a weight-assignment method based on the resilience features being considered and, more so, on the system parameters, such as topology and size of the generating assets, which vary greatly from one system to another. Therefore, it becomes very difficult to assess which system parameters might be more dominant towards increasing/decreasing resilience, thereby making it difficult to assign weights to the multitude of resilience features that can be considered. Thus, weight-assignment methods are typically subjective and depend on the system operator's interpretation. On the other hand, in this paper, we propose a method that is a step towards objective quantification of a system's resilience by removing any subjective weight assignment requirement. This entails that an unsupervised method is used to condense a vector to a number where there is no or minimal input for weights. In the proposed SOM-based approach, the neurons learn the various simulated system states and the corresponding resilience feature values, and then arrange themselves automatically in a one-dimensional array based on the learnt relative importance of those features.

Apart from developing the resilience metric, few studies explore making planning/operational decisions to improve the metric. Reference [13] develops a framework incorporating time-varying customer damage functions to size the generating assets and then select the nodes and the type of load to be supplied to reduce the system outage cost. In [14], a resilient scheduling framework consisting of a resource optimization stage, an economic dispatch stage, and a fault restoration stage is developed to improve the system resilience. A resource-constrained unit commitment framework for integrated electrical and natural gas systems is adopted in both [15] and [16] to enhance resilience, where, essentially, the minimum resource availability is constrained based on the criterion of being able to supply critical loads for some time based on solar irradiance and load forecasts. Further, [17] and [18] propose models to accommodate random outages in integrated energy systems by optimizing topology and the number of loads to be restored.

These studies mainly focus on either system planning or a resource-constrained approach for operational resilience improvement; however, in case of the disconnection of an energy source due to power line damages, how to make full use of the available reserves and how to coordinate different resources to ensure reliable and resilient operation is still challenging and needs further study. Thus, for improved system performance under extreme events, there should be a holistic integration of resilience in operational decision making instead of simply considering the resilience requirements in the planning stage or the resource-constrained approach in the operation stage.

Therefore, in addition to developing the SomRes technique for resilience quantification, this paper develops a novel resilient operation strategy to improve critical load survivability under extreme event scenarios. This is achieved using a convex optimization model to find not only the optimal dispatch decisions of generation sources but also the optimal allocation of energy reserves using the transportation network and the optimal topology configuration. The main contributions of this paper are as follows:

1) A novel resilience quantification method is proposed to consider relevant static as well as dynamic parameters of the system and to estimate time-varying resilience by anticipating how the static/dynamic system parameters will affect critical load survivability. This method is a step towards objective quantification of a system's resilience as it eliminates the need for the system operator to perform any subjective weight assignment, which can be erroneous as it depends on human's interpretation.

2) The proposed method considers a wide range of system parameters that could potentially affect critical load survivability in an event, compared to some existing works, which only consider either the topological aspects of the system and ignore the power flow aspect, or consider the power flow aspect but ignore the transportation network aspect. Also, SOM can be trained offline, and the well-trained SOM model enables that resilience can be estimated fast and in real time by simply finding the neuron which is closest to the system features at that time.

3) Different from existing studies which mainly opt for a resource-constrained approach for resilience improvement, this paper proposes a novel resilient-operation control algorithm that incorporates resilience directly as a feedback in the optimization model to enhance the survivability of critical loads in extreme event scenarios. To the best of the authors' knowledge, an approach explicitly maximizing estimated resilience has not been studied so far in the literature. Further, most studies ignore the transportation network to enable optimal flow of energy reserves, which has been modeled in this paper for maximizing operational resilience.

The rest of this paper is organized as follows. Section II presents the SomRes technique to evaluate resilience; Section III presents the distribution system operation strategy under extreme events incorporating resilience and optimal resource allocation; Section IV presents the numerical simulation results and discussion; and Section V provides concluding remarks.

## II. SomRes (Resilience Quantification Using Self-Organizing Maps)

### A. SOM based on forced training of neurons

SOM [19] is an unsupervised, competitive-learning neural network and has been extensively used in the artificial intelligence literature to cluster data without having prior knowledge of the class memberships of the input data or their relative importance. These properties of SOM make it an ideal candidate to aggregate and condense a vector of features to a scalar value without using any form of weight assignment inputs, and thus has been adopted in this paper as an aggregation method.

To obtain a scalar value, i.e., resilience index, for a given set of features, i.e., resilience parameters in Section II-B), a one-dimensional SOM-based resilience quantification approach, SomRes, is proposed as shown in Fig. 1. To this end, SOM is first trained with features for several system states, and each

This article has been accepted for publication in a future issue of this journal, but has not been fully edited. Content may change prior to final publication. Citation information: DOI 10.1109/TSG.2022.3150226, IEEE Transactions on Smart Grid



system state (with its corresponding set of features) maps itself onto a specific neuron. This one-dimensional array of neurons can then be considered as a scale representing resilience, $\mathfrak{R}$, ranging from 0 to 1 and can be written as follows:

$$\mathfrak{R} = \mathcal{SOM}(r_{ae}, r_{cl}, r_{gd}, r_{rl}, r_{cs}, r_{er}, r_{sub}, r_{path}) \quad (1)$$

where, $r_{ae}$ represents the average asset-level resilience; $r_{cl}$ the sustainability of critical loads; $r_{gd}$ the capacity and geographical distribution of DERs; $r_{rl}$ the criticality of power lines; $r_{cs}$ the cyber-security of automation infrastructure; $r_{er}$ the availability of energy reserves; $r_{sub}$ the feasible islands; and $r_{path}$ the path redundancy. Details about the definitions and formulations of these parameters are provided next.

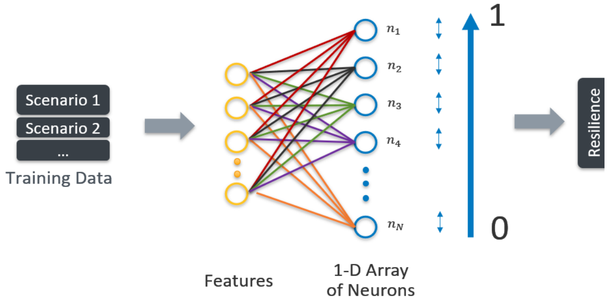


Fig. 1. Schematic of the SOM-based resilience quantification.

*B. Parameters affecting resilience*

Many parameters affecting resilience have been mentioned in recent publications from federal and private organizations [20]-[22]. The following eight distribution system parameters are down selected based on their relative importance in improving a system's resilient operation capabilities, and their mathematical models are developed by this paper. Also, it is noted that a wide variety of other resilience-relevant parameters can be included in the proposed SomRes technique, subject to the availability of data.

*(1) Static parameters*

These parameters are considered static since they remain mostly time-invariant over short operational timescales.

(1.a) Average asset-level resilience: A major factor affecting system-level resilience is the sturdiness and robustness of the generation assets inside a distribution system and can be related to the environmental rating provided by the manufacturer of the asset regarding water, wind, or heat damage thresholds. This environmental rating can be quantified using a value, $r_{a,i}$, ranging from 0 to 1, and the average asset-level resilience ($r_{ae}$) can then be calculated:

$$r_{ae} = \sum_{i \in N} r_{a,i} / n(N) \quad (2)$$

where $N$ is the set of nodes in the considered distribution system section, and $n(N)$ denotes the number of nodes.

(1.b) Cybersecurity of Automation Infrastructure: As power systems evolve toward the increased integration of automation and control, cybersecurity of the automation infrastructure forms an important aspect of the system's resilience capabilities in dealing with and mitigating the effects of cyberattacks; therefore, the cybersecurity parameter for resilience quantification can be considered as a value $r_{cs}$ on a scale depicting the level of security protocols.

(1.c) Capacity and geographic distribution of DERs: If DERs of sufficient capacity are geographically spread throughout the distribution system, they could provide power to a large number of critical load nodes, even in the scenario of an event damaging parts of the distribution grid. On the contrary, a geographic area with a concentrated cluster of DERs is less likely to support most of the critical load nodes if an event were to isolate that area itself; therefore, the parameter $r_{gd}$ calculates the geographic diversity of generation compared to that of the load nodes. The higher the diversity of generation, the higher the chances of survival of the loads if an event happens.

$$r_{gd} = \frac{div_g}{div_l} \quad (3)$$

$$div_g = \frac{\sum_{i \in N} \sum_{j \in N, j \neq i} \hat{g}_i \hat{g}_j \, d_{g_{ij}}}{\sum_{i \in N} \sum_{j \in N, j \neq i} \hat{g}_i \hat{g}_j \, \hat{d}_{g_{ij}}} \quad (4)$$

$$div_l = \frac{\sum_{i \in N} \sum_{j \in N, j \neq i} \hat{l}_i^c \hat{l}_j^c \, d_{l_{ij}}}{\sum_{i \in N} \sum_{j \in N, j \neq i} \hat{l}_i^c \hat{l}_j^c \, \hat{d}_{l_{ij}}} \quad (5)$$

$$d_{g_{ij}} = \sqrt{\left(x_{g_i} - x_{g_j}\right)^2 + \left(y_{g_i} - y_{g_j}\right)^2} \quad (6)$$

$$d_{l_{ij}} = \sqrt{\left(x_{l_i} - x_{l_j}\right)^2 + \left(y_{l_i} - y_{l_j}\right)^2} \quad (7)$$

$$\hat{d}_l = \max_{i,j} d_{l_{ij}} \,, \qquad \hat{d}_g = \max_{i,j} d_{g_{ij}} \quad (8)$$

where $div_g$ and $div_l$ denote the geographic diversity of generation assets and load nodes, respectively; $d_{g_{ij}}, d_{l_{ij}}$ denote the distance between nodes $i$ and $j$, and $\hat{d}_g, \hat{d}_l$ denote the maximum distance among all nodes for generation assets and load nodes, respectively; and $x_{g_i}, y_{g_i}, x_{l_j}, y_{l_j}$ are the geographic x and y coordinates of the generator $i$ and load $j$.

(1.d) Criticality of power lines: The criticality of power lines between generation and load nodes needs to be defined to quantify the effect of critical line failures; therefore, the parameter $r_{rl}$ quantifies the criticality of paths as follows:

$$r_{rl} = 1 - \sum_{i \in N} \sum_{j \in N, i \neq j} \frac{\sum_{k \in P(i,j)} E(L_k(i,j)) \times [u_k(i,j) - 1]}{E(P(i,j))} \quad \ldots (9)$$

where $L_k(i,j)$ is the line $k$ of the path $P(i,j)$ between generator $i$ and load $j$; $E(\cdot)$ is the electrical distance; and $u_k(i,j)$ is the number of times the line $L_k(i,j)$ is used for all $P(i,j)$. In (10), the right side of the equation captures how much overlap of lines exists in the possible paths between generators and loads. If a line $L_k(i,j)$ is used only once for all possible path combinations, $u_k(i,j)$ will be 1, meaning that the line is not critical. However, if multiple path combinations use the line $L_k(i,j)$, $u_k(i,j)$ will be greater than 1, meaning that the line is more critical, leading to a reduced $r_{rl}$.

*(2) Dynamic parameters:*

These parameters are considered dynamic since they are time-variant over operational timescales.

(2.a) Sustainability of critical loads: Critical loads are the loads to which an uninterrupted power supply is expected to be maintained under all circumstances. The continuity of power supply is ensured by using DERs, such as DG, PV, and BESS; therefore, the parameter $r_{cl}$ captures whether the existing generation capability is enough to enable the survival of critical loads for at least T time steps.

$$r_{cl} = 1 - \sum_{t\in T} \left\{ \frac{\sum_{i\in N}[l_i^c(t) - g_i(t)]}{\mathrm{T}\sum_{i\in N} l_i^c(t)} \right\} \quad (10)$$

where $t$ is used to index time slots over the horizon $T = \{\tau, \tau + 1 \dots, \tau + \mathrm{T}\}$, $l_i^c(t)$ is the critical load at the node $i$, and $g_i(t)$ is the total generation at the asset at node $i$.

(2.b) Availability of energy reserves: During and after an extreme event, the presence of enough energy reserves, such as diesel for DG and the remaining SOC of BESS, will ensure that the distribution system can sustain until the damaged lines are repaired; therefore, the presence of such reserves and their optimal utilization by the control system significantly affects resilience.

$$r_{er} = \sum_{t\in T} \left\{ \frac{\sum_{i\in N}[d_i(t) - f_i g_i(t)]_+}{\mathrm{T}\sum_{i\in N} f_i g_i(t)} + \frac{\sum_{i\in N}[b_i(t) - \eta_i p_{bi}(t)]_+}{\mathrm{T}\sum_{i\in N} \eta_i p_{bi}(t)} \right\} \quad (11)$$

where $d_i(t)$ is the available diesel at DG $i$ at time $t$, and $f_i$ is the factor relating the diesel consumption of the DG to its power generation; $b_i(t)$ is the SOC of the BESS $i$ at time $t$, $\eta_i$ is the BESS efficiency, and $p_{bi}(t)$ is the BESS active power. Essentially, the right side of (11) calculates whether there is sufficient diesel and energy storage available for the DG and the BESS to be dispatched.

(2.c) Feasible islands: A distribution system with switching devices has the capability to form multiple islands with geographically diverse DERs and loads, thereby improving its resilience against an event. And the number and location of switching devices determines the number of possibly feasible islands that can be formed. The feasibility of such islands can be described in terms of sufficient generation capacity available in each island, voltage limits, etc.; therefore, the parameter $r_{sub}$ captures the number of feasible islands possible relative to the total number of generation asset nodes in the system.

$$r_{sub} = \frac{\sum_{t\in T} \arg\max_{N_{sub}} \sum_{j\in\{1,..N_{sub}\}} \left\{ \begin{array}{c} \left[\sum_{i\in N_j}\left(g_{ij}(t) - l_{ij}^c(t)\right)\right]_+ + \\ \sum_{i\in N_j}\left[v_{max} - v_{ij}(t)\right]_+ \\ + \sum_{i\in N_j}\left[v_{ij}(t) - v_{min}\right]_+ \end{array} \right\}}{T\, n(N)} \quad \dots (12)$$

where $N_{sub}$ is the number of independent islands possible; $N_j$ is the set of nodes in the island $j$; and $g_{ij}$, $l_{ij}^c$, and $v_{ij}$ are the generation, critical load, and voltage at node $i$ of island $j$.

(2.d) Path redundancy: The higher the number of possible paths from DERs to loads is, the higher is the likelihood of ensuring power supply to such loads under varied damage scenarios of an event; thus, the normalized value of possible parallel paths (with the switches closed) available from a generator node to a critical load node is used as another parameter, $r_{path}$, affecting resilience and is defined as:

$$r_{path} = \frac{\sum_{j\in N}\sum_{i\in N} 1\Big/\sum_{k\in K} E\big(P_k(i,j)\big)}{n(N)^2\Big/2\hat{E}\big(P_k(i,j)\big)} \quad (13)$$

where $P_k(i,j)$ is the $k^{th}$ path from node $i$ to $j$; and $E\big(P_k(i,j)\big)$ and $\hat{E}\big(P_k(i,j)\big)$ are the electrical distance of the path and the maximum electrical distance, respectively.

### *C. Resilience quantification*

(*Assumption-1*) It is assumed that the DSO has access to time-granular system data, such as present topology of the system, actual generation asset capacities and load requirements, location and quantity of energy reserves, etc., to be able to estimate the system's time-varying resilience. The inputs required by the DSO and the relevant feature outputs are presented in Table I.

The SOM in its basic form, however, is not suitable for resilience quantification because the mapping of inputs to the neurons might not be smooth and might not follow a uniform gradient throughout; therefore, the following modifications are made for the proposed SomRes approach:

- The edge neurons are forced to learn two systems: an imaginary system with the best characteristics that would make it the most resilient and another imaginary system with the worst characteristics that would make it the least resilient. For example, the most resilient system could be one having a sufficient capacity of DERs at each load node, a robust decentralized control system, etc. The least resilient system could be one having no DERs and that depends fully on the bulk power source, an unreliable bulk grid, high critical load requirement, and so forth.
- For SOM training using $\mathrm{N_S}$ neurons, the initial value of the neighborhood function starts with the value $N_s$ and shrinks gradually as the iterations progress, based on a Gaussian distribution. This means that, initially, the influence zone of each neuron is the entire array of $\mathrm{N_S}$ neurons, and as the SOM gets iteratively trained, the shrinking influence zones of the neurons will train the neurons to learn a smooth gradient mapping of the input data.

Table I. Input/Output List for Resilience Quantification

| Parameters | Inputs | Output |
|---|---|---|
| Asset-level resilience | Asset environmental ratings | $r_{ae}$ |
| Cybersecurity of Automation Infrastructure | Security protocols | $r_{cs}$ |
| Capacity and geographic distribution of DERs | Location and size of generation assets and loads | $r_{gd}$ |
| Criticality of power lines | Network topology | $r_{rl}$ |
| Sustainability of critical loads | Critical loads and DER generation capability, and their forecasts | $r_{cl}$ |
| Availability of energy reserves | Location and SOC of BESS, location and amount of diesel | $r_{er}$ |
| Feasible islands | Network topology, critical loads and DER generation capability, and their forecasts | $r_{sub}$ |
| Path redundancy | Network topology, DER generation and load nodes | $r_{path}$ |
| Resilience metric | $r_{ae}, r_{cs}, r_{gd}, r_{rl}, r_{cl}, r_{er}, r_{sub}, r_{path}$ | $\mathfrak{R}$ |

As shown in Fig. 2, training the SOM while forcing edge neurons results in a smoother heatmap and can be used effectively for resilience quantification. After the SOM

This article has been accepted for publication in a future issue of this journal, but has not been fully edited. Content may change prior to final publication. Citation information: DOI 10.1109/TSG.2022.3150226, IEEE Transactions on Smart Grid



training, any distribution system—not previously used for training and with its own set of input parameters for which resilience is to be determined—will map itself onto a certain neuron matching with the new system's parameters evaluated as in Section II-B. As an example, suppose the new system maps onto the neuron, $n$, with neuron 1 considered to have a resilience 0, whereas neuron $N_S$ is considered to have a resilience 1; thus, the resilience of the system will be in the range $\left({}^{N_S-n}/_{N_S}, {}^{N_S-n+1}/_{N_S}\right)$, and we then calculate the system resilience metric as follows:

$$\Re = \frac{N_S - n + 0.5}{N_S} \tag{14}$$

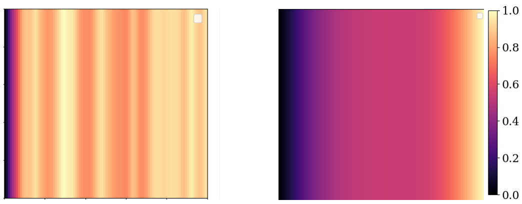


(a) (b)

Fig. 2. SOM heat map without (a) and with (b) forced training of edge neurons.

## III. Distribution System Operation Integrating Resilience and Resource Allocation

For low-probability but high-consequence disaster events, distribution utilities presently have very few options to manage and mitigate the effects of an event while the event is still unfolding. Even after the disaster event, it can take utilities a huge amount of time to restore power completely. For example, in the destruction aftermath of Hurricane Maria in 2017, the electricity supply in Puerto Rico was completely restored after almost one year; therefore, strategies have been proposed in the literature to use DERs along with network reconfiguration to supply the critical loads for the longest possible period. During such disaster events, however, when many distribution lines along with roads in the transportation network could be damaged, there might be significant critical load shedding if the resources—such as the SOC of BESS or diesel for DG are not dispatched proactively. Further, critical load shedding can be significantly reduced if the resources are allocated with the explicit aim of enhancing resilience.

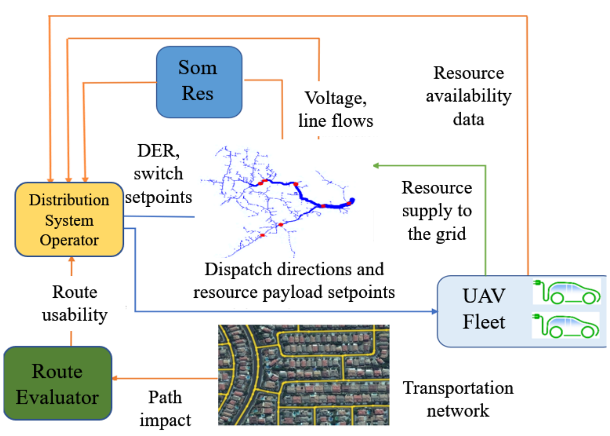


Fig. 3. Proposed resource allocation framework.

In this paper, we consider that UAVs can be dispatched among the DG nodes to transport diesel; thus, optimally allocating diesel resources can help meet critical load demands in areas isolated by the event by proactively dispatching UAVs to provide efficient, reliable, and critical load support during the disaster event. Further, the SOC of BESS is optimally managed in this paper by proactively charging and discharging the BESS; therefore, this section presents an integrated power and resource allocation strategy in which the UAVs are optimally dispatched along with DER optimization and network reconfiguration to enhance the distribution system's survivability and resilience. Importantly, the proposed strategy also considers real-time resilience that is quantified using SomRes as a feedback in the system optimization, as shown in Fig. 3.

### *A. Distribution grid and transportation network modeling*

For the distribution grid network model, $i \in N$ is used to denote multiphase buses, and we consider the grid network to have one PCC with the distribution feeder, thereby indexing the PCC as bus 0. The set of non-PCC buses is denoted as $N^+ := N\backslash\{0\}$; $a, b, c$ denotes the three phases; and $\Phi_i$ is the set of phases of bus $i$ such that $\Phi_i \in \{a, b, c\}$. Also, $p := [p_i^\phi, \phi \in \Phi_i, i \in N^+]$, $q := [q_i^\phi, \phi \in \Phi_i, i \in N^+]$ ,and $v := [v_i^\phi, \phi \in \Phi_i, i \in N^+]$ denote the active power consumption vector, the reactive power consumption vector, and the squared voltage magnitudes vector, respectively. Using this notation, we employ the distribution power flow model presented in [23], also shown in (15a), where $\tilde{v}_0 := [v_0^\phi]$ represents the squared voltage magnitudes at the phases of the PCC. Each element of the matrices $R$ and $X$ is defined in (15b)–(15d), where $i_\psi$ denotes the $\psi$ phase of bus $i$; $j_\phi$ the $\phi$ phase of bus $j$; $z_{\xi\zeta}^{\psi\phi}$ the impedance of the common path between nodes $i$ and $j$ leading up to the PCC; $Re$ and $Im$ denote the real and imaginary parts, respectively; and $\overline{x}$ denotes the complex conjugate of $x$ ($\phi, \psi = 0,1,2$ are used to calculate phase differences):

$$v = Rp + Xq + \tilde{v}_0 \tag{15a}$$

$$R(i_\psi, j_\phi) = \partial_{p_j^\phi} v_i^\psi = -2Re\left\{\overline{Z}_{ij}^{\psi\phi} e^{-\frac{\mathrm{i}2\pi(\psi-\phi)}{3}}\right\} \tag{15b}$$

$$X(i_\psi, j_\phi) = \partial_{q_j^\phi} v_i^\psi = +2Im\left\{\overline{Z}_{ij}^{\psi\phi} e^{-\frac{\mathrm{i}2\pi(\psi-\phi)}{3}}\right\} \tag{15c}$$

$$Z_{ij}^{\psi\phi} := \sum_{(\xi,\zeta)\in E_i \cap E_j} z_{\xi\zeta}^{\psi\phi} \tag{15d}$$

(*Assumption-2*) This paper assumes that the nodes of the transportation network are the same as the nodes of the grid network, with the edges of the transportation network corresponding to the roads. But we recognize the difference between real transportation networks and grid networks, and we will incorporate realistic transportation network models in our future work.

In the considered transportation network, multiple roads might be connected to a node $n \in N$. Let each road connecting a node $n$ be denoted as $r_n^i$, where $i$ indexes the set of connected roads; therefore, roads connected to a node $n$ can be written as $r_n^1, r_n^2, r_n^3, \ldots$. Further, assume that at each time step $t$, $dn_{r^i}^t$ denotes the amount of diesel sent out from node $n$ to the $i^{th}$ road; therefore, for each node $n$, the following equations hold:

$$dn_{r^i}^t = dn_{r^i}^t \quad , \qquad if\ dn_{r^i}^t > 0 \tag{16a}$$

This article has been accepted for publication in a future issue of this journal, but has not been fully edited. Content may change prior to final publication. Citation information: DOI 10.1109/TSG.2022.3150226, IEEE Transactions on Smart Grid



$$dn_{r^i}^{\max(t+1,\lambda^{r^i})} = dn_{r^i}^t, \quad if\ dn_{r^i}^t < 0 \tag{16b}$$

where $\lambda^{r^i}$ denotes the time delay or the time required for the UAV when using the road $r^i$ to reach the other node. The equation (16a) ensures that if the diesel is being sent out, i.e., $dn_{r^i}^t > 0$, it is considered in the current time step itself; however, if the diesel is to be received at the node *n*, i.e., $dn_{r^i}^t < 0$, there is a maximum time delay of $\lambda^{r^i}$ for the diesel to be considered, given that the UAV takes a time $\lambda^{r^i}$ to reach the node *n*.

Also, for the diesel dispatch using UAV between any two connected nodes *m* and *n*, the following equation ensures that the diesel is deducted from one node and is added to the other node:

$$dn_{r^i}^t = -dm_{r^j}^t\ , \quad \forall\,(m,n) \in T_e\ , r^i = r^j \tag{17}$$

where $T_e$ is the set of roads in the transportation network.

*B. Resource allocation and resilient operational dispatch*

For optimal resource allocation, it is assumed that only diesel can be transported via the UAVs. This assumption can be easily extended to include portable BESS or DG transportation, but it has not been considered in this paper. For each node having a DG, the initial diesel availability is denoted as $D_n^0$, and the diesel availability at each time-step *t* is denoted as $D_n^t$. *t* increments by 1 at each 15-min interval. Further, let $dn_0^t$ denote the diesel self-consumption of the DG at node *n* to produce the active power $p_{n,0}^t$; therefore, for each node *n* with DG, the following equation calculates the diesel availability at time *t*, i.e., $D_n^t$:

$$D_n^t = D_n^0 - dn_0^t - \sum_i dn_{r^i}^t \tag{18}$$

Further, for each DG, it is assumed that the active power generation ($p_{n,0}^t$) follows a concave relationship with the amount of diesel consumed, and it is represented in the following equation:

$$dn_0^t = a * \left(p_{n,0}^t\right)^2 + b * p_{n,0}^t + c \tag{19}$$

where *a*, *b*, and *c* are constants for the DG.

Then, the following presents the resilient operation dispatch strategy adopted by the DSO to be able to supply critical loads during extreme events.

*(1) Optimization problem for DGs*

The cost involved in the transportation of diesel from one DG node to another and the diesel consumption in the DG itself is considered in the following objective function for each DG node *n*:

$$f_{dg} = \sum_{t\in T}\left\{\gamma_{dg}\left[a\left(p_{n,0}^t\right)^2 + bp_{n,0}^t + c\right] + \sum_{r^i} \lambda^{r^i} {dn_{r^i}^t}^2\right\} \tag{20}$$

where $\gamma_{dg}$ is a weighting factor, the first term denotes the quadratic formulation (19) of diesel consumption in the DG and the second term denotes the penalty for importing/exporting diesel. The objective function (20) for each DG node *n*, $f_{dg}$ , is subject to the following constraints:

$$D_n^t \geq 0 \tag{21a}$$

$$p_{n,0}^{min} \leq p_{n,0}^t \leq p_{n,0}^{max} \tag{21b}$$

$$0.1 * D_n^t \leq dn_{r^i}^t \leq D_n^t, if\ dn_{r^i}^t > 0 \tag{21c}$$

where $p_{n,0}^{max}$ and $p_{n,0}^{min}$ are the maximum and minimum power output capability of the DG *n*. Eq. (21c) ensures that if diesel is being sent out, a minimum 10% is assumed to be sent while limiting the sent diesel to be what is currently present at node *n*, i.e., $D_n^t$.

*(2) Optimization problem for load nodes*

Each load node is assumed to be operated by a LEMS managing behind-the-meter DERs, such as an electric water heater and a heating, ventilating, and air-conditioning appliance. For the load node *n*, a flexibility-band, along with a nominal power, is considered to be reported by LEMS at that load node to the DSO. This flexibility band can be evaluated based on the critical load requirement and the comfort preferences of the owner. The design of the LEMS is based on [24] and is omitted in this paper for brevity. The flexibility band reported by the LEMS at node *n* consists of lower and upper bounds of active/reactive powers $p_{n,\vee}^t, q_{n,\vee}^t, p_{n,\wedge}^t, q_{n,\wedge}^t$, along with nominal powers $p_{n,*}^t, q_{n,*}^t$; therefore, the objective function presented in (22) aims to deviate as little as possible from the nominal LEMS powers, but load-shedding is also considered if the lower bound (which denotes the critical load requirement at that node) is not sufficient for the system constraints:

$$\begin{aligned} f_l = \sum_{t\in T}\Big\{&\gamma_{pl}\left(p_{n,*}^t - p_n^t\right)^2 + \gamma_{ql}\left(q_{n,*}^t - q_n^t\right)^2 \\ &+ \gamma_{ps} \max_{\forall n} p_{n,shed}^t \\ &+ \gamma_{qs} \max_{\forall n} q_{n,shed}^t\Big\} \end{aligned} \tag{22}$$

where $\gamma_{pl}, \gamma_{ql}, \gamma_{ps}, \gamma_{qs}$ are weighting factors; $p_{n,shed}^t$ and $q_{n,shed}^t$ are active/reactive load shedding variables; and $p_n^t, q_n^t$ denote optimal active/reactive powers. The first two terms minimize deviations of optimal active/ reactive powers ($p_n^t, q_n^t$) from the nominal LEMS powers, and the last two terms minimize active/reactive load shedding.

The objective $f_l$ for each load node *n* is subject to the following power limit constraints:

$$p_{n,\vee}^t - p_{n,shed}^t \leq p_n^t \leq p_{n,\wedge}^t \tag{23a}$$

$$q_{n,\vee}^t - q_{n,shed}^t \leq q_n^t \leq q_{n,\wedge}^t \tag{23b}$$

$$p_{n,shed}^t \geq 0, q_{n,shed}^t \geq 0 \tag{23c}$$

*(3) Optimization problem for PV-BESS*

We assume that each load node also has a PV system and a BESS installed, and the optimization problem for a PV-BESS system at node *n* is presented as:

$$\begin{aligned} f_{pb} = \sum_{t\in T}\Big\{&\left[\gamma_{pv,p}\left(p_{pv,n}^t - p_{pv,n,0}^t\right)^2 + \gamma_{pv,q}\left(q_{pv,n}^t\right)^2\right] \\ &+ \left[\gamma_{cycle}\left(p_{bat,n}^t - p_{bat,n}^{t+1}\right)^2\right] \\ &+ \gamma_b\left({p_{ch,n}^t}^2 + {p_{dis,n}^t}^2\right. \\ &\left.+ {q_{bat,n}^t}^2\right)\Big\} \end{aligned} \tag{24a}$$

where $\gamma_{pv,p}, \gamma_{pv,q}, \gamma_{cycle}, \gamma_b$ are weighting factors; $p_{pv,n}^t, q_{pv,n}^t$ denote the optimal active/reactive power output of the PV system; and $p_{ch,n}^t, p_{dis,n}^t, q_{bat,n}^t$ denote the optimal charging, discharging and reactive power, respectively, of the BESS. The first and second terms minimize PV active power curtailment and reactive power usage, respectively; the third term aims to reduce cycling of the BESS; and the fourth term ensures that

This article has been accepted for publication in a future issue of this journal, but has not been fully edited. Content may change prior to final publication. Citation information: DOI 10.1109/TSG.2022.3150226, IEEE Transactions on Smart Grid



simultaneous charging and discharging are penalized along with reducing reactive power usage.

The objective (24a) is subject to the constraints:

$$p_{ch,n}^{t} + p_{dis,n}^{t} = p_{bat,n}^{t} \qquad (24b)$$

$$0 \le p_{ch,n}^{t} \le \ p_{bat,max}^{n} \qquad -p_{bat,max}^{n} \le p_{dis,n}^{t} \le 0 \qquad (24c)$$

$$S_{bat,n}^{t+1} = S_{bat,n}^{t} + \Delta T\left(\alpha_{ch} p_{ch,n}^{t} + \frac{p_{dis,n}^{t}}{\alpha_{dis}}\right) \qquad (24d)$$

$$\left(p_{bat,n}^{t}\right)^{2} + \left(q_{bat,n}^{t}\right)^{2} \le \ (I_{bat}^{n})^{2} \qquad (24e)$$

$$S_{min}^{n} \le S_{bat,n}^{t} \le S_{max}^{n} \qquad (24f)$$

where $p_{bat,max}^{n}$ is the power rating of the BESS; $S_{bat,n}^{t}$ is the SOC at time *t*; $\alpha_{ch}$ and $\alpha_{dis}$ are the charging/discharging efficiencies of the BESS; $I_{bat}^{n}$ is the BESS converter rating; and $S_{min}^{n}$ and $S_{max}^{n}$ are the minimum/maximum allowable SOC values.

*(4) Optimization problem for switches*

For switches, $s_{ij}$, in the network, the following objective function penalizes frequent switching actions in the horizon *H*:

$$f_s = \sum_{ij \in Lines} \sum_{t \in T} \gamma_s \left\{ b_{s,ij}^{t} - b_{s,ij}^{t-1} \right\}^2 \qquad (25a)$$

$$subject\ to: \qquad \widetilde{\boldsymbol{P}} = -\widetilde{\boldsymbol{P}}^{\boldsymbol{T}}, \widetilde{\boldsymbol{Q}} = -\boldsymbol{Q}^{\boldsymbol{T}} \qquad (25b)$$

$$\widetilde{\boldsymbol{P}}\boldsymbol{1}^{\boldsymbol{T}} = \widetilde{\boldsymbol{Q}}\boldsymbol{1}^{\boldsymbol{T}} = 0, \quad , \qquad \check{A}^{T} \le \boldsymbol{b}_s^t \le \hat{A}^{\boldsymbol{T}} \qquad (25c)$$

$$-M\boldsymbol{b}_s^t \le \widetilde{\boldsymbol{P}} \le M\boldsymbol{b}_s^t \quad , \ -M\boldsymbol{b}_s^t \le \widetilde{\boldsymbol{Q}} \le M\boldsymbol{b}_s^t \qquad (25d)$$

where $\gamma_s$ is a weighting factor and $b_{s,ij}^{t}$ denotes the binary value of the switch $s_{ij}$; $\boldsymbol{1}$ is the column vector of ones; $\boldsymbol{b}_s^t$ is the adjacency matrix including actual switch statuses $b_{s,ij}^{t}$; $\check{A}$ and $\hat{A}$ are adjacency matrices with all switches off and on respectively; $\widetilde{\boldsymbol{P}}$ and $\widetilde{\boldsymbol{Q}}$ are matrices with diagonal elements representing nodal power injections and off-diagonal elements representing line power flows; and *M* is a very large number. It is noted that the presence of a faulty line is automatically considered by the adjacency matrices $\check{A}$ and $\hat{A}$ , which will vary over time depending on how the propagation of an extreme event alters the system graph.

(*Assumption 3*) It is noted that there must be switches in a real-world power network that must be operated to isolate the faults. However, we would like to note that fault isolation is out of scope of this paper and hence, determining which switches need to be operated to isolate the faults has not been considered. Further, the proposed method can be applied to systems with different topologies and since the operation of switches to isolate the faults will simply lead to a different system topology, therefore, for simplicity and to maintain focus on the proposed method, the lines impacted by an event are simply considered to be out of service. And we consider that the DSO uses this modified topology information to update matrices $\check{A}$ and $\hat{A}$.

*(5) System-level optimization problem*

The system-level optimization problem to be solved by the DSO constitutes a social welfare formulation of objectives and constraints of DG, LEMS, PV, BESS and switches, along with system-level constraints such as voltage limit and power-balance constraints. Further, as discussed in Section I about the present need for a resilient operation control strategy, we incorporate resilience as feedback to the system-level optimization problem. This is accomplished by simultaneously maximizing the SomRes resilience index $\mathfrak{R}$; however, because the parameters in Section II-B and the SomRes itself are highly non-linear, a linear regression to approximate the SomRes value is needed to maintain the convexity of the system-level problem.

Since the DSO will solve the system-level optimization problem on operational timescales, the static parameters presented in (2)-(9) will not change significantly and are therefore not considered in the operational resilience maximization; instead, only the dynamic parameters presented in (10-(13) are considered. The nonlinear SomRes resilience index $\mathfrak{R}$ can be written in terms of the control variables as follows:

$$\mathfrak{R} = SOM\{b_s^t, dn_0^t, dn_{r^i}^t, p_n^t, q_n^t, p_{n,shed}^t, q_{n,shed}^t, p_{pv,n,0}^t, p_{bat,n}^t\} \quad \ldots (26a)$$

The SomRes index can therefore be linearized with respect to the aforementioned variables as follows:

$$\widetilde{\mathfrak{R}} = [\pi_1^t, \pi_2^t, \ldots]\big[b_s^t, dn_0^t, dn_{r^i}^t, p_n^t, q_n^t, p_{n,shed}^t, q_{n,shed}^t, p_{pv,n,0}^t, p_{bat,n}^t\big]' \qquad (26b)$$

where $\widetilde{\mathfrak{R}}$ is the approximated SomRes resilience index, $\pi_i^t$ is the coefficient for the variable index *i* for time *t*, and $[\cdot]'$ is the transpose operator.

Thus, the overall system-level optimization problem for the DSO to solve can be formulated as follows:

$$\begin{aligned}
\min \mathcal{F}_{DSO} = & \sum_{n \in Ng} \sum_{t \in T} \left\{ \gamma_{dg}\left[a\left(p_{n,0}^t\right)^2 + b p_{n,0}^t + c\right] + \sum_{r^i} \lambda^{r^i} {dn_{r^i}^t}^2 \right\} \\
& + \sum_{n \in Nl} \sum_{t \in T} \begin{Bmatrix} \gamma_{pl}\left(p_{n,*}^t - p_n^t\right)^2 + \gamma_{ql}\left(q_{n,*}^t - q_n^t\right)^2 \\ +\gamma_{ps} \max\limits_{\forall n} p_{n,shed}^t + \gamma_{qs} \max\limits_{\forall n} q_{n,shed}^t \end{Bmatrix} \\
& + \sum_{n \in Nl} \sum_{t \in T} \begin{Bmatrix} \left[\gamma_{pv,p}\left(p_{pv,n}^t - p_{pv,n,0}^t\right)^2 + \gamma_{pv,q}\left(q_{pv,n}^t\right)^2\right] \\ +\left[\gamma_{cycle}\left(p_{bat,n}^t - p_{bat,n}^{t+1}\right)^2\right] \\ +\gamma_b\left({p_{ch,n}^t}^2 + {p_{dis,n}^t}^2 + {q_{bat,n}^t}^2\right) \end{Bmatrix} \\
& + \sum_{s \in S} \sum_{t \in T} \gamma_s \{b_s^t - b_s^{t-1}\}^2 - \widetilde{\mathfrak{R}} \qquad (27a)
\end{aligned}$$

*subject to:* (15a)-(15d), (16a)-(16b), (17)-(19), (21a)-(21c), (23a)-(23c), (24b)-(24f), (25b)-(25d), (26b).

$$\sum_{n \in N} \{p_n^t\} \le 0 \qquad (27b)$$

$$\sum_{t \in T} \sum_{n \in N} [V_{min} - V_n^t]_+^2 + [V_n^t - V_{max}]_+^2 = 0 \qquad (27c)$$

where $V_{min}, V_{max}$ denote the minimum/maximum allowable voltages. The constraint (27b) ensures that power balance is maintained in the distribution system, whereas constraint (27c) maintains node voltages within the upper/lower limits. $Ng$ and $Nl$ are the total number of DGs and load nodes respectively.

## IV. Simulation Results and Discussion

In this section, the proposed SomRes method is employed to evaluate system resilience, and then the estimated resilience is used in the resource allocation and restoration algorithm to control the distribution network and DERs with resilience as a perspective. The IEEE 123-bus test system is used for simulation and the line parameters data have been adopted from [25]. In addition, as shown in Fig. 4, it is assumed that the distribution system is installed with 25 kW PV and 25 kW/40 kWh BESS systems at several nodes (in orange) along with 100 kW of DGs across 12 nodes (in orange and green) to improve the system performance during extreme events.

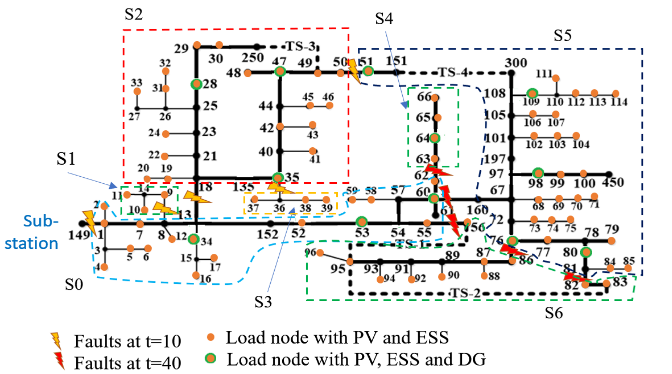


Fig. 4. Single line diagram of the 123-bus test system, showing locations of installed PV, BESS, DGs, along with subnetworks formed under the worst case fault scenario.

We assume that the resource allocation and restoration strategy in (27) is executed at a 15-min time granularity, and an extreme event that moves through the modified IEEE 123-bus test system follows a path such that it creates multiple open-line faults during a period of 2 days (i.e., 192 time-steps of 15-min duration each), thereby finally dividing the system into several subnetworks. These subnetworks are also depicted in Fig. 4. Note in Fig. 4 that one set of faults occurs at *t=10* and the other set at *t=40*; thus, the analysis can be divided into three sets of time-periods – *0-9*, *10-39*, and *40-192* – and the corresponding areas in the figures are shaded *white*, *light blue* and *light grey*, respectively. Note also that the proposed strategies do not forecast the propagation of an event. Instead, only when an event comes to realization, the proposed strategies consider the affected lines, assuming that the DSO has knowledge of the affected lines instantly.

Further, the optimization problem was set up in a Python environment using the well-known commercially available solver CPLEX from IBM [26] integrated with the optimization package *cvxpy* [27] and the simulation studies were conducted on a 4.0 GHz Intel-i7 processor.

### *A. Resilience-neutral vs resilience-enhanced strategy*

To verify the effectiveness of the proposed SomRes technique and the resource allocation-based restoration strategy, two scenarios were simulated and programmed. In the first scenario,

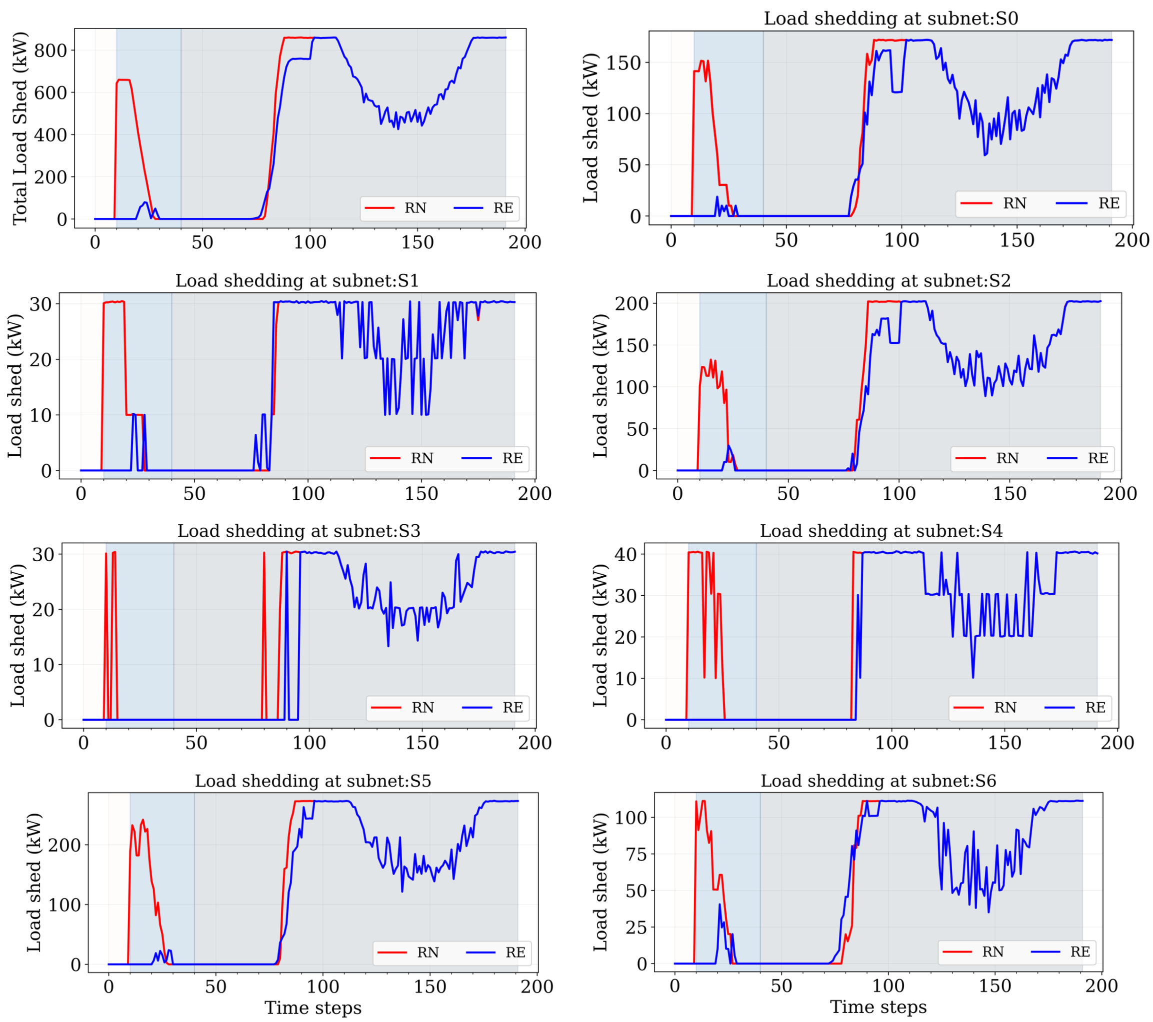


Fig. 5. Total system load-shed (top-left figure) and load-shed in each subnetwork for RN and RE scenarios.

named resilience-neutral (RN) resource-allocation based restoration, the resilience estimate $\widetilde{\mathfrak{R}}$ is removed from the optimization model (27); whereas in the second scenario, named resilience-enhanced (RE) resource-allocation based restoration, the resilience estimate $\widetilde{\mathfrak{R}}$ is considered in the optimization model. Both scenarios have a rolling optimization horizon $T$ of 96 time-steps.

Fig. 5 shows the time-series results for the total system load-shed in the RN and RE scenarios. It is observed that the total load shed in the RN scenario is 21,069 kWh, and in the RE scenario it is 18,603 kWh; thus, with the resilience-enhanced resource allocation-based restoration strategy, the load shedding is reduced significantly by 2,466 kWh or 11.7%.

As mentioned previously, because the considered event path will eventually divide the system into seven subnetworks, we also analyze the dispatch of resources in these subnetworks. Fig. 5 shows the time-series results of the load shed in these subnetworks, and in the following, we analyze in detail the difference between the RN and RE scenarios.

*(1) Time-steps t=0-9:*

As shown in Fig. 4, the event strikes the distribution system at t=10, so for t=0-9, the system is operating in a normal condition. In the RN scenario, the DSO does not proactively prepare for any imminent extreme event and continues operating normally by using the resources present in the system. Because there is no solar irradiance present during these time steps, the DSO uses an optimal combination of BESSs and DGs to support the loads, as shown in Fig. 6, which shows the plots for total PV, BESS and DG power generation. However, compared to the RN scenario, the RE scenario proactively charges the BESSs during t=0 to 9, as shown in the 'BESS powers' and 'Total BESS SOC' plots. The RE scenario also results in a net import of power from the distribution substation at node 149, as seen in the 'Generation & Critical Load' plot, to optimally conserve its resources to prepare for the extreme event. Further, the RE scenario also enables proactive optimal dispatch of diesel fuel required for DGs.

Fig. 7 and Fig. 8 show plots for the RN and RE scenarios for reserve availability (diesel fuel and BESS SOC, respectively) with respect to per unit critical load requirement. The "reserves per unit critical load" of each subnetwork calculates the ratio of diesel fuel or BESS SOC that are accessible to load nodes in that subnetwork over the critical load requirement for the optimization horizon T. As shown in Fig. 7(a), the RE scenario determines that all the fuel needs to be allocated to the DGs in subnetwork S2, which will improve the factors contributing to resilience and the resilience index itself. In the RN scenario, however, the DSO does not transfer any diesel proactively, as shown in Fig. 7(b). As a result, as shown in Fig. 9 which presents resilience parameters and the resilience index, the combined behavior of the proactive charging of BESSs and diesel allocation in the RE scenario results in a significant increase in parameters $r_{er}, r_{path}$ and $r_{cl}$ between t=0-9, meaning that the loads now have better and robust access to energy resources. The parameter $r_{sub}$ does not change for the RE scenario during this time, but it is higher than that of the RN scenario, because the RE scenario managed to secure access to resources proactively to be able to form multiple islands with sufficient generation capability in them if an extreme event were to strike.

*(2) Time-steps t=10-39:*

At t=10, when the extreme event first strikes, the subnetworks S1, S2 and S3 are isolated from the rest of the system, whereas subnetworks S0, S4, S5 and S6 are still

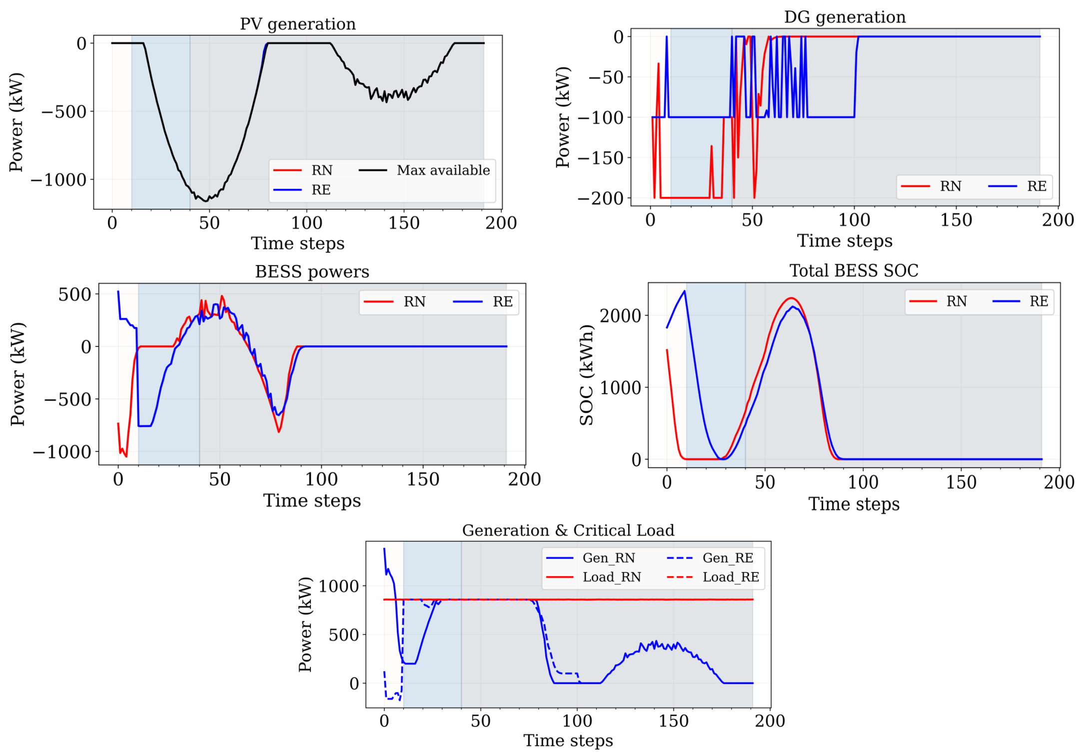


Fig. 6. Plots for total PV, DG and BESS powers, BESS SOC, along with total generation and load plots.

This article has been accepted for publication in a future issue of this journal, but has not been fully edited. Content may change prior to final publication. Citation information: DOI 10.1109/TSG.2022.3150226, IEEE Transactions on Smart Grid



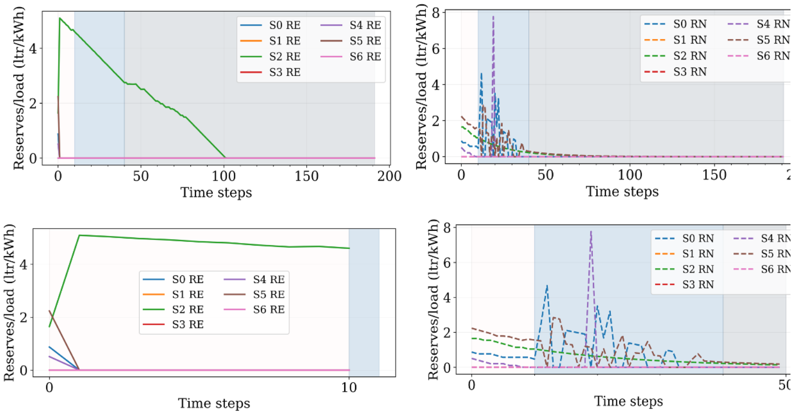


Fig. 7. Diesel fuel allocation plots for RE and RN scenarios.

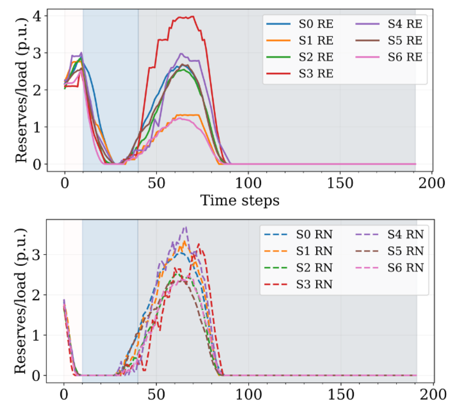


Fig. 8. BESS SOC allocation plots for RE and RN scenarios.

connected to each other. In this paper, we consider an important assumption that the isolated subnetworks cannot exchange any diesel fuel with other isolated subnetworks or the rest of the system because of the damaged transportation network. This assumption is similar to the no power flow possibility among such isolated subnetworks. Thus, in the RN scenario, because the system was not prepared for the event, Fig. 7 (b) shows that there is a significant exchange of diesel fuel among S0, S4 and S5 because they are still connected, and the transportation system is assumed to be intact; however, no fuel exchange occurs with S2 because it has become isolated after t=10. Note that the other isolated subnetworks during this time, namely S1 and S3, do not have any DG and therefore do not exchange any fuel. Overall, as shown in Fig. 5, this results in significant load-shedding in the RN scenario in the initial time-steps of this period when there is no solar irradiance available. After approximately t=20, when solar irradiance becomes available, the load shedding in the RN scenario gradually decreases.

Fig. 9 shows that the resilience index falls dramatically in the RE scenario at the beginning of this time period, whereas it remains at low for the RN scenario. For the RE scenario, this reduction is due to the damage to the system and the reduction in available reserves, whereas for the RN scenario, the lack of proactive resource allocation subsequently led to almost full discharge of the BESSs and the use of DGs led to fuel shortages (shown in Figs. 6, 7 and 8); however, as the PV systems start generating power, there is sufficient generation availability to charge the BESSs from *t=29* (see Fig. 6 'BESS powers' and 'Total BESS SOC' plots) and thus the resilience index starts increasing.

*(3) Time-steps t=40-192:*

At t=40, the extreme event causes further damage to the distribution system, and it results in all the subnetworks to become completely isolated from each other and now they can exchange neither power nor fuel with each other. It is also seen in Fig. 7 that at the start of this time-period, the RN scenario has less diesel left per unit critical load compared to the RE scenario due to reasons mentioned in previous time-steps. Therefore, the main source of energy generation in the RN scenario for the subnetworks are the PV+BESS systems, as seen in Fig. 6 where DGs provide power only during the first few time steps and the rest of the critical load is being supplied by PVs. Similarly, in the RE scenario, PV+BESS systems provide most of the power to the critical loads; however, in contrast to the RN scenario, there is a relatively higher amount of diesel left per unit of critical load requirement (as shown in Fig. 7(a)), which helps in a reduced load-shedding (as shown in Fig. 5).

This property is also depicted in Fig. 9 "Reserves/load" plot, which shows that overall, the average reserve availability per critical load over all the nodes for the RE scenario remains higher than that for the RN scenario. Consequently, the critical loads are supplied for longer (until *t=101*) in the RE scenario as compared to the RN scenario where the critical loads are supplied only until *t=86*. Further, once the reserves are fully exhausted in the RE and RN scenarios, no BESS charging is observed when PV generation begins at *t=112* due to insufficient solar irradiance which now only supports a subset of critical loads.

Based on this analysis, it can be concluded that the significant difference in load shedding between RN and RE scenarios is because the resilient strategy optimally allocates diesel resources and SOC of BESSs by not just considering the present system state but also the possibility of a worst-case scenario, thereby enabling critical load survivability under uncertainties. This leads to an optimal resource allocation which improves the chances of loads to survive during an extreme event. The RE and RN strategies also make use of network reconfiguration by turning on and off (denoted as 1 and 0) the tie-switches TS-1 through TS-4, as depicted in Fig. 10 (a) and (b).

## *B. Statistical Analysis*

Until now, we analyzed the outperformance of a resilience-enhanced resource-allocation and restoration strategy versus a resilient-neutral strategy considering a pre-defined event scenario. As resilience is a concept based on optimum preparation for and mitigation of worst-case events, we also analyze the statistical performance of the proposed RE strategy by considering different event and outage scenarios. Essentially, we use Monte-Carlo simulation to generate a variety of branch damage scenarios, and then the total critical load shed is evaluated for each scenario.

As shown in Fig. 11, to generate branch damage scenarios, graph reduction was first performed by keeping only the active nodes (with either loads or with generating sources) and eliminating the remaining passive nodes in the chosen 123-bus system. Assuming the remaining lines after graph reduction are

This article has been accepted for publication in a future issue of this journal, but has not been fully edited. Content may change prior to final publication. Citation information: DOI 10.1109/TSG.2022.3150226, IEEE Transactions on Smart Grid



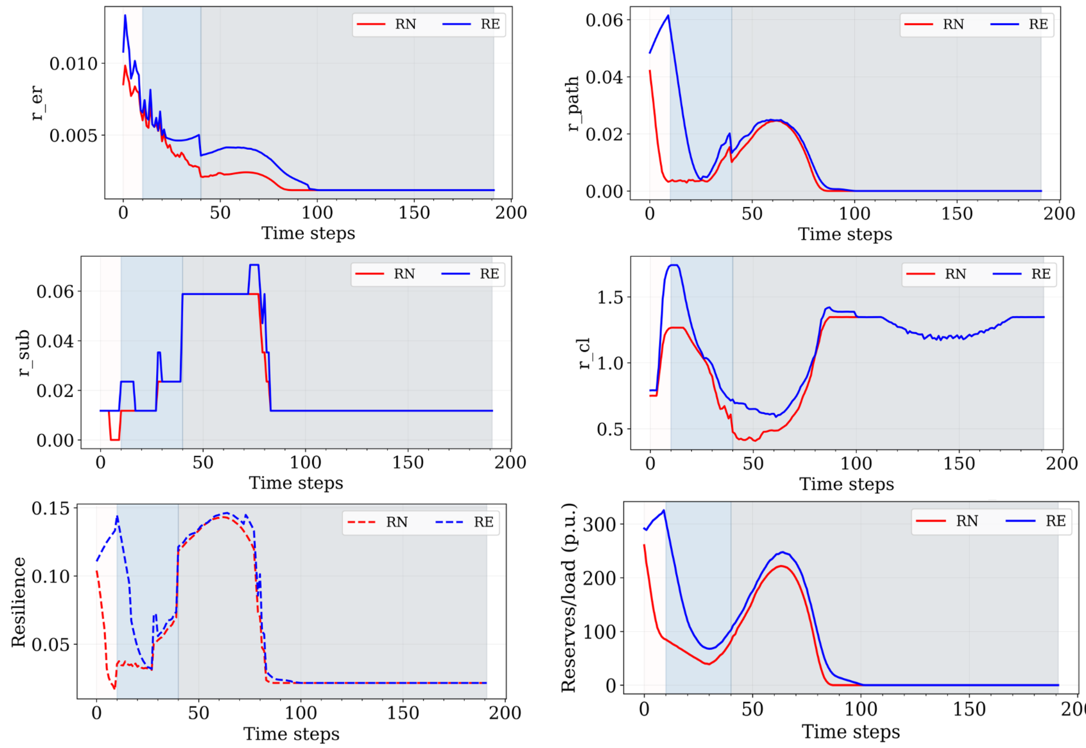


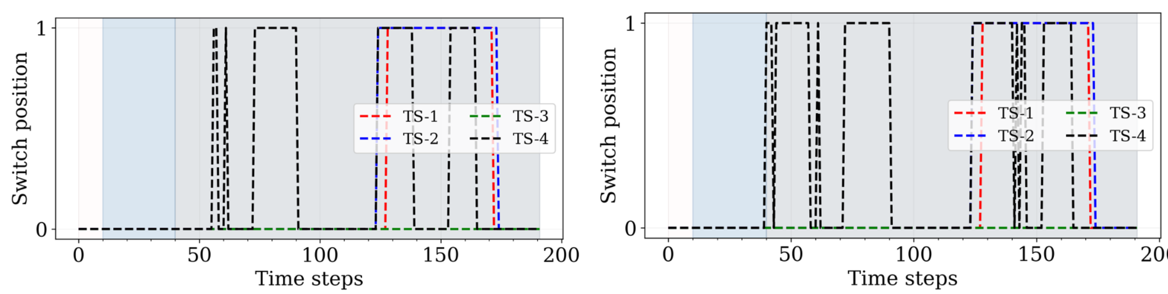


Fig. 10. (a) Tie switch positions for the RN scenario and (b) for the RE scenario.

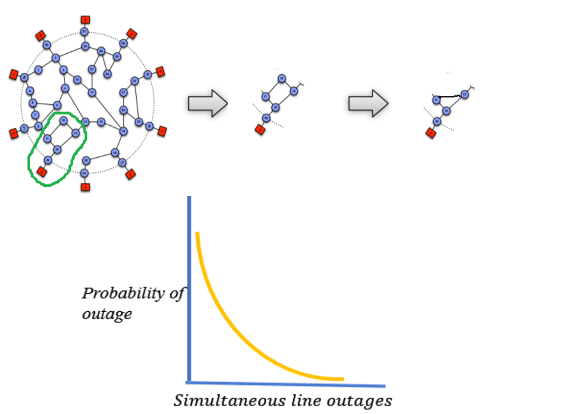


Fig. 11. Figures showing graph reduction method (top) and the probability curve chosen for line outages (bottom).

$\tilde{n}$, the number of combinations of possible line outages is $2^{\tilde{n}} - 1$. Simulating all such line outages, however, is computationally prohibitive; therefore, we simulated a fraction '$k$' of the possible outage combinations as given in the following equation:

$$\sum_{r'=\tilde{n}-r}^{r'=\tilde{n}} p_{r'} \frac{\tilde{n}!}{r'! \times (\tilde{n}-r')!} \leq k \times (2^{\tilde{n}} - 1) \qquad (28)$$

where $r$ is the value denoting a set of simultaneous line outages; $p_{r'}$ is the probability distribution given in Fig. 11 (bottom figure) for $r'$; and ! is the factorial operator. Choosing a fixed value $k$ will provide us with the value $r'$. Using this method, 10,000 line outage scenarios were generated, and the critical energy shed in each scenario was evaluated.

Further, the 10,000 scenarios were generated for five cases, and they were simulated using the RN and RE strategies, as explained in Section III. The five cases are as follows – Case-1: No diesel dispatch allowed via UAVs with optimization horizon T=1 time step; Case-2: RN scenario with optimization horizon T=24 time-steps; Case-3: RE scenario with optimization horizon T=24 time-steps; Case-4: RN scenario with optimization horizon T=96 time steps; Case-5: RE scenario with optimization horizon T=96 time steps. The results of the five cases are summarized in the box plots presented in Fig. 12, which shows that the proposed RE strategy has a significant performance advantage over the RN strategy in

This article has been accepted for publication in a future issue of this journal, but has not been fully edited. Content may change prior to final publication. Citation information: DOI 10.1109/TSG.2022.3150226, IEEE Transactions on Smart Grid



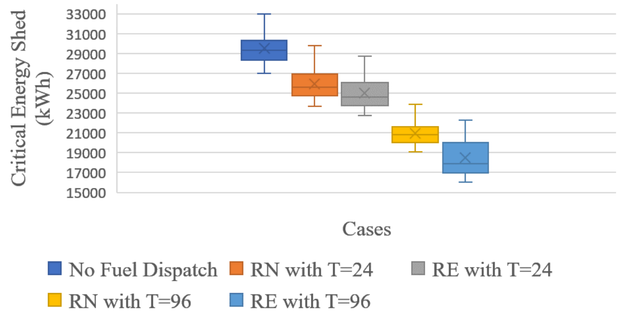


Fig. 12. Box plot for critical energy shed during the 2-day period.

terms of reducing critical load shedding. Further, the optimization horizon is also seen to play a significant role, and with a longer optimization horizon, both the RN and RE strategies can better manage the charging/ discharging of BESS considering PV and critical load forecasts to reduce critical load shedding.

## C. Resilience heatmap

As mentioned previously, SomRes can be used to quantify the resilience index of a system and help distribution utilities identify different survival capabilities of their networks during extreme events. Taking the seven subnetworks shown in Fig. 4 as examples, we can analyze each of these subnetworks as if they were separate entities. This survival capability is then quantified using the resilience index SomRes, as presented in Section-II, for each subnetwork, and the average SomRes resilience quantified over time for each subnetwork for the RE scenario is depicted in Fig. 13. Each subnetwork is color-coded from yellow (most resilient) to purple (almost non-resilient) based on the SomRes index.

The resilience heatmap depicted in Fig. 13 suggests that the presence of appropriate quantities of generation sources, such as DGs, PVs and BESSs can provide significant resilience enhancement if BESS SOC and diesel fuel are managed and dispatched appropriately to support critical loads.

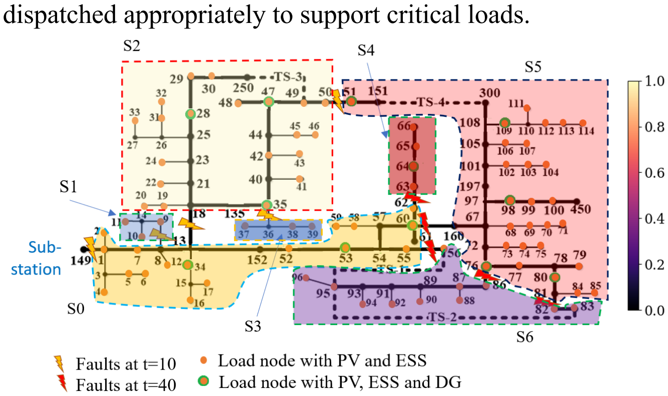


Fig. 13. Heat map showing the average resilience quantification of each subnetwork.

## D. SOM Benchmarking

In this section, performance of the proposed SOM-based resilience quantification approach is compared with two other feature aggregation methods – 1) a simple numerical average of the features; and 2) the state-of-the-art CI-based method. Further, the three resilience quantification approaches (average-based, SOM-based, and CI-based) are compared with the normalized critical energy supplied to the system.

To this end, the four resilience feature time-series plots evaluated for the RE scenario in Section IV-A – i.e., “r_er”, “r_path”, “r_sub”, and “r_cl” plots for RE in Fig. 9 – are considered for calculating the time-varying aggregation plots for the feature average and the CI methods (the time-varying resilience plot for the SOM-based method is already presented in Fig. 9 corresponding to these four features).

For the CI-based aggregation of the features, there is also a subjective weight assignment required for the non-additive (or fuzzy) measure $\mu$ to compute the following discrete integral:

$$CI = \int f\, d\mu = \sum_{i=1}^{4} [f(x_i) - f(x_{i-1})]\, \mu(A_i) \qquad (29)$$

where $f(x_i)$ indicates that the features have been permuted so that $0 \le f(x_1) \le \cdots f(x_4) \le 1$ and $A_i = \{x_i, \ldots x_4\}$. The measures $\mu(A_i)$ are set as follows – $\mu(x_i) = 0.1$; $\mu(x_i x_j) = 0.45$; $\mu(x_i x_j x_k) = 0.55$; and $\mu(x_1 x_2 x_3 x_4) = 0.9$.

Further, to benchmark the three aggregation approaches, the normalized critical energy that can be served needs to be computed for each time-step $t$. This normalized critical energy that can be served at time-step $t$ is essentially the summation of the critical energy served for $S$ event scenarios based on the state of the system at time $t$. This is explained as follows:

- For each time-step t, obtain the state of the system $\psi^t$, i.e., present network topology, location and availability of diesel and SOC reserves, forecasted generation outputs, and forecasted critical load requirement.

$$\psi^t = [\boldsymbol{b}_s^t, D_n^t, S_{bat,n}^t, p_{n,\vee}^{t,\ldots}, p_{pv,n,0}^{t,\ldots}] \qquad (30)$$

- Using the state vector $\psi^t$ as the initialization state, generate $S = 100$ scenarios denoting the possible propagation paths of an event through the 123-bus system (for example, one such scenario has been discussed in Section IV-A).
- For each such scenario $s \in S$, run the optimization problem (27) and calculate the critical energy that can be supplied, and finally compute the normalized energy supplied over all the S scenarios.

$$C^t = \sum_{s \in S} \sum_{t'=t}^{T} p_n^{s,t'} \Big/ \sum_{s \in S} \sum_{t'=t}^{T} p_{n,\vee}^{s,t'} \qquad (31)$$

The comparison of the critical energy served $C^t$ with the three aggregation metrics is shown in Fig. 14, and it can be seen that the SOM plot has a closer trend to the critical energy served plot as compared to the average and the CI plots.

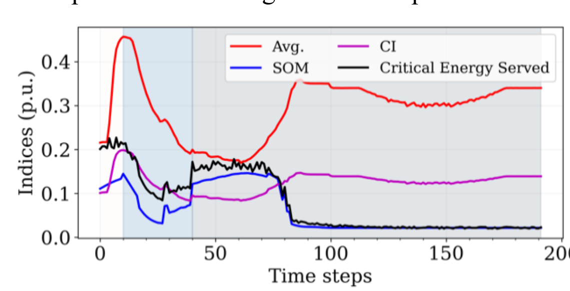


Fig. 14. Benchmarking of the SOM-based resilience quantification approach.

Indeed, when covariances of each of the three aggregation metrics are calculated, the SOM plot is observed to have a positive correlation with the critical energy served with a covariance value of 0.003219, while the average and the CI plots have covariances of -0.001965 and -0.000418, respectively. This shows that weight assignment plays an important role in both the weighted-sum approach (of which average is a special case) as well as the CI-based approach, and an arbitrary weight assignment (as done here) can affect these aggregation methods significantly. On the other hand. the SOM-based resilience quantification approach does not require any subjective weight assignment and therefore results in a better estimate of system resilience.

### *E. Computation runtime and scalability considerations*

It is noted that the optimization problem presented in Section III is modelled as a mixed-integer convex formulation and various commercial or open-source solvers can be utilized to determine optimal solutions faster. In this paper, we use the CPLEX solver [26] from IBM. For the mixed-integer optimization problem formulated for the 123-bus system, the CPLEX solver took approx. 9.7 seconds to solve for each time-step. Further, since the optimization model utilizes model-predictive control, the need for detailed stochastic formulations was removed. Stochastic formulations might have also resulted in a higher computation time per time-step compared to the current model-predictive deterministic approach.

Further, the proposed SOM-based resilience quantification method as well as the resilient operation optimization problem can be applied to larger systems, such as the 8500-bus system, either through a fully centralized control of all the 8500-buses or through a hierarchical control of subnetworks within the larger system as it might result in some computational burden benefits. The authors are currently exploring the proposed SOM-based method on a large distribution feeder in Colorado, US, and the results will be discussed in a future work.

## V. Conclusions

To enable the system operators to embed resilience in their operational decision makings, this paper first proposes a novel SOM-based resilience quantification method, named as SomRes, to estimate the resilience index of distribution systems. SomRes is an objective quantification of a system's resilience as it eliminates the need for the system operator to perform any subjective weight assignment, which can be erroneous as it depends on human's interpretation. Using SomRes, a convex mixed-integer model-predictive resource-allocation and resilient operation model is further developed to optimally dispatch mobile UAVs and BESS powers in conjunction with optimizing PVs, DGs and network topology to minimize load-shedding and maximize system resilience. Simulation studies on the IEEE 123-bus test system show that the proposed SomRes quantification method correlates well with the criterion of normalized critical energy served compared to benchmark approaches. Further, the proposed resilient resource allocation and dispatch strategy significantly reduces critical load shedding compared to a dispatch strategy without resilience embedded as feedback in the optimization. Overall, the SomRes quantification method and the resilient dispatch strategy can be used by system operators, when an extreme event is imminent and while it is unfolding, to prepare for and adapt the system's resources dynamically to achieve the goal of maintaining power supply to the critical loads.

## References

[1] Vugrin, Eric D., Castillo, Andrea R, and Silva-Monroy, Cesar Augusto. Resilience Metrics for the Electric Power System: A Performance-Based Approach. United States: N. p., 2017. Web.

[2] National Academies of Sciences, Engineering, and Medicine. 2017. Enhancing the Resilience of the Nation's Electricity System. Washington, DC: The National Academies Press.

[3] Grid Modernization Laboratory Consortium (GMLC). "Grid Modernization: Metrics Analysis (GMLC1.1) Reference Document, Version 2.1." U.S. Department of Energy, May 2017.

[4] P. J. Maliszewski and C. Perrings, "Factors in the resilience of electrical power distribution infrastructures," Appl. Geogr., vol. 32, no. 2, pp. 668–679, 2012.

[5] Ouyang M, Dueñas-osorio L (2014) Multi-dimensional hurricane resilience assessment of electric power systems.

[6] P. Bajpai, S. Chanda and A. K. Srivastava, "A Novel Metric to Quantify and Enable Resilient Distribution System Using Graph Theory and Choquet Integral," in IEEE Transactions on Smart Grid, vol. 9, no. 4, pp. 2918-2929, July 2018, doi: 10.1109/TSG.2016.2623818.

[7] Kwasinski, A. Quantitative Model and Metrics of Electrical Grids' Resilience Evaluated at a Power Distribution Level. Energies 2016, 9, 93.

[8] Yanling Lin, Zhaohong Bie, Tri-level optimal hardening plan for a resilient distribution system considering reconfiguration and DG islanding, Applied Energy, Volume 210, 2018, Pages 1266-1279, ISSN 0306-2619, doi.org/10.1016/j.apenergy.2017.06.059.

[9] S. Ma, B. Chen and Z. Wang, "Resilience Enhancement Strategy for Distribution Systems Under Extreme Weather Events," in IEEE Transactions on Smart Grid, vol. 9, no. 2, pp. 1442-1451, March 2018, doi: 10.1109/TSG.2016.2591885.

[10] K. Anderson et al., "Integrating the Value of Electricity Resilience in Energy Planning and Operations Decisions," in IEEE Systems Journal.

[11] C. Lv, H. Yu, P. Li, K. Zhao, H. Li and S. Li, "Coordinated Operation and Planning of Integrated Electricity and Gas Community Energy System With Enhanced Operational Resilience," in IEEE Access, vol. 8, pp. 59257-59277, 2020, doi: 10.1109/ACCESS.2020.2982412.

[12] Y. Li, Z. Li, F. Wen and M. Shahidehpour, "Minimax-Regret Robust Co-Optimization for Enhancing the Resilience of Integrated Power Distribution and Natural Gas Systems," in IEEE Transactions on Sustainable Energy, vol. 11, no. 1, pp. 61-71, Jan. 2020, doi: 10.1109/TSTE.2018.2883718.

[13] Y. Wang, L. Huang, M. Shahidehpour, L. L. Lai, H. Yuan and F. Y. Xu, "Resilience-Constrained Hourly Unit Commitment in Electricity Grids," in IEEE Transactions on Power Systems, vol. 33, no. 5, pp. 5604-5614, Sept. 2018, doi: 10.1109/TPWRS.2018.2817929.

[14] M. Yan, Y. He, M. Shahidehpour, X. Ai, Z. Li and J. Wen, "Coordinated Regional-District Operation of Integrated Energy Systems for Resilience Enhancement in Natural Disasters," in IEEE Transactions on Smart Grid, vol. 10, no. 5, pp. 4881-4892, Sept. 2019, doi: 10.1109/TSG.2018.2870358.

[15] Y. Wang et al., "Coordinating Multiple Sources for Service Restoration to Enhance Resilience of Distribution Systems," in IEEE Transactions on Smart Grid, vol. 10, no. 5, pp. 5781-5793, Sept. 2019, doi: 10.1109/TSG.2019.2891515.

[16] J. C. Whitson and J. E. Ramirez-Marquez,"Resiliency as a component importance measure in network reliability," Rel. Eng. Syst. Safety, vol. 94, no. 10, pp. 1685–1693, 2009.

[17] S. Chanda and A. K. Srivastava, "Defining and Enabling Resiliency of Electric Distribution Systems With Multiple Microgrids," in IEEE Transactions on Smart Grid, vol. 7, no. 6, pp. 2859-2868, Nov. 2016, doi: 10.1109/TSG.2016.2561303.

[18] Emre Yamangil, Russell Bent, and Scott Backhaus. 2015. Resilient upgrade of electrical distribution grids. In Proceedings of the Twenty-Ninth AAAI Conference on Artificial Intelligence (AAAI'15). AAAI Press, 1233–1240.

[19] T. Kohonen, "The self-organizing map", Proceedings of the IEEE, vol. 78, no. 9, 1990.

[20] https://www.rand.org/pubs/research_reports/RR883.html

This article has been accepted for publication in a future issue of this journal, but has not been fully edited. Content may change prior to final publication. Citation information: DOI 10.1109/TSG.2022.3150226, IEEE Transactions on Smart Grid



[21] https://www.nap.edu/catalog/24836/enhancing-the-resilience-of-the-nations-electricity-system
[22] https://www.osti.gov/biblio/1481633-analysis-microgrid-locations-benefitting-community-resilience-puerto-rico
[23] K. Utkarsh, F. Ding, C. Zhao, H. Padullaparti and X. Jin, "A Model-Predictive Hierarchical-Control Framework for Aggregating Residential DERs to Provide Grid Regulation Services," 2020 IEEE Power & Energy Society Innovative Smart Grid Technologies Conference (ISGT), Washington, DC, USA, 2020, pp. 1-5, doi: 10.1109/ISGT45199.2020.9087773.
[24] P. Munankarmi, X. Jin, F. Ding and C. Zhao, "Quantification of Load Flexibility in Residential Buildings Using Home Energy Management Systems," American Control Conference (ACC), Denver, CO, USA, 2020, pp. 1311-1316.
[25] The IEEE 123-node test feeder. [Online]. Available: https://site.ieee.org/pestestfeeders/resources
[26] https://www.ibm.com/analytics/cplex-optimizer
[27] S. Diamond, & S. Boyd, "CVXPY: A Python-embedded modeling language for convex optimization", The Journal of Machine Learning Research, 17(1), 2909-2913.

**Kumar Utkarsh** is a Research Engineer with the Power Systems Engineering Center at the National Renewable Energy Laboratory (NREL). He was previously with Robert Bosch South-East Asia Pvt. Ltd. as a Research Scientist. He received his B.Tech. degree from the Indian Institute of Technology (IIT-BHU), India, and his Ph.D. degree from the National University of Singapore, Singapore, in 2011 and 2018, respectively, in Electrical & Computer Engineering. His research interests are in micro-grid and smart-grid energy management systems, distributed energy resource integration studies, frequency/voltage stability, generation/demand side management, and power system resilience quantification and enhancement.

**Fei Ding** received her B.S. and M.S. degrees from Tianjin University, China, in 2008 and 2010, respectively, and her Ph.D. degree from Case Western Reserve University, Cleveland, OH, USA in 2014. Now she is a Distinguished Member of Research Staff and Senior Research Engineer at the National Renewable Energy Laboratory (NREL). Her research interests include renewable energy grid integration, distributed energy resources aggregation and controls, grid resilience and security. She is leading multiple projects at NREL on developing advanced models and controls for managing grid-edge resources to enhance grid flexibility, reliability, and resilience, and developing new advanced distribution management system and distributed energy resource management system applications to modernize emerging distribution grids.